Fast and Slow Steps in the Activation of Sodium Channels

CLAY M. ARMSTRONG and WM. F. GILLY

From the Department of Physiology, G4, School of Medicine, University of Pennsylvania, Philadelphia, Pennsylvania 19104

ABSTRACT Kinetic features of sodium conductance (g_{Na}) and associated gating current (I_g) were studied in voltage-clamped, internally perfused squid axons. Following a step depolarization I_g ON has several kinetic components: (*a*) a rapid, early phase largely preceding g_{Na} turn-on; (*b*) a delayed intermediate component developing as g_{Na} increases; and (*c*) a slow component continuing after g_{Na} is fully activated. With small depolarizations the early phase shows a quick rise (<40 μs) and smooth decay; the slow component is not detectable. During large pulses all three components are present, and the earliest shows a rising phase or initial plateau lasting ~80 μs. Steady-state and kinetic features of I_g are minimally influenced by control pulse currents, provided controls are restricted to a sufficiently negative voltage range. I_g OFF following a strong brief pulse also shows a rising phase. A depolarizing prepulse producing g_{Na} inactivation and I_g immobilization eliminates the rising phase of I_g OFF. g_{Na}, the immobilized portion of I_g ON, and the rising phase reappear with similar time-courses when tested with a second depolarizing pulse after varying periods of repolarization. 30 mM external $ZnCl_2$ delays and slows g_{Na} activation, prolongs the rising phase, and slows the subsequent decay of I_g ON. Zn does not affect the kinetics of g_{Na} tails or I_g OFF as channels close, however. We present a sequential kinetic model of Na channel activation, which adequately describes the observations. The rapid early phase of I_g ON is generated by a series of several fast steps, while the intermediate component reflects a subsequent step. The slow component is too slow to be clearly associated with g_{Na} activation.

INTRODUCTION

The molecular events that regulate opening and closing of Na channels in axon membrane are driven by the rearrangement of charged gating structures in response to a change of membrane potential. Movement of these charged structures generates a detectable "gating current" (Armstrong and Bezanilla, 1973, 1974; Keynes and Rojas, 1973, 1974; Meves, 1974). Thus far, gating current associated with Na activation has been observed, but nothing unequivocally related to the other major gating processes in axons, Na inactivation or K activation, has been found.

Previous studies concentrating on the relation between activation and

J. GEN. PHYSIOL. © The Rockefeller University Press · 0022-1295/79/12/0691/21 $1.00 691
Volume 74 December 1979 691-711

inactivation have led to the conclusion that the two processes are not independent. Inactivation is not associated with detectable gating current and is thought to derive its voltage sensitivity from coupling to activation; i.e., inactivation can occur only after activation of a channel is nearly complete (Armstrong and Bezanilla, 1977; Bezanilla and Armstrong, 1977; Meves and Vogel, 1977 *a*,*b*). A similar conclusion had been reached from studies of the kinetics of the g_{Na} (Hoyt, 1968; Goldman and Schauf, 1972).

We turn here to a study of the kinetic features of gating current with the aim of learning more about the activation process. Activation involves a number of steps and gating current reflects all of them, giving information that cannot be obtained from studying conductance changes alone. Important information about the steps that lead to opening of the channel is contained in the first 100 μs of the gating current transient. This interval is close to the limits of time resolution and has proved difficult to study. The Hodgkin and Huxley equations (1952) predict an instantaneous rise and exponential decay for gating currents. Most published records, on the other hand, show an instantaneous jump in the current, followed by either a plateau or a rise to a peak.

Is this "rising phase" a machine artifact or the result of nonlinear charge movement during the control pulses? We have examined these questions experimentally and conclude that the rising phase probably originates from neither of these sources but is instead a genuine feature of gating current and gives information about the relative transition rates among closed states of the channel. Perhaps, more importantly, we also demonstrate a relatively slow component of gating current that had previously escaped detection. This component can be seen clearly for steps positive to about −20 mV, and probably arises from the last and slowest step in activation, the actual opening of the channel.

METHODS

Experiments were performed on isolated giant axons of *Loligo pealii*, obtained at the Marine Biological Laboratory, Woods Hole, Mass. Cleaned axons were internally perfused and voltage clamped. Except for minor changes, the techniques were the same as those described in Bezanilla and Armstrong (1977). The changes were as follows: (*a*) The internal electrode was not a "piggy-back." Instead, an axial wire was inserted by one manipulator, and a voltage pipette (containing an electrically floating Pt wire) was inserted from the same cut end of the axon by another manipulator. This had the minor advantage that none of the surface of the axial wire was covered with glue. (*b*) Pulses were generated by a 12-bit D/A converter interfaced to the computer. (*c*) The current measuring region of the chamber in most experiments was 6.2 mm rather than 3.1 mm. This seemed to improve the signal-to-noise ratio appreciably.

In order to prevent saturation of the amplifiers and A/D converter by the very large surge of capacity current following a voltage step, a linear transient proportional in amplitude to the voltage step applied was subtracted from the membrane capacity current transient. The combined signal was then fed to an integrating input stage (Bezanilla and Armstrong, 1977), digitized by a 12-bit A/D converter with a sample interval of 10 μs, and then fed to a sample and hold amplifier. 720 samples were taken

per sweep; the last 600 points were compressed 5 to 1, giving one point per 50 μs. Most of the records shown were obtained with the P/4 procedure (Armstrong and Bezanilla, 1974). Some traces were digitally filtered by replacing the n^{th} sample point, I_n, by the sum $(I_n/2) + (I_{n-1} + I_{n+1})/4$.

Performance of the clamp and the recording apparatus for a step input of current is shown in Fig. 1 *a*. The step shown was generated by a voltage clamp pulse applied to a resistor. The rise time of the recorded signal was ~20 μs.

Tests were performed on model membranes of two types in checking the linearity of the system: (*a*) a purely resistive "membrane" made simply from a resistor or (*b*) a capacitor. Cancellation of the signal from either resistor or capacitor (assuming ideality) should have been perfect using the P/4 procedure. In fact, cancellation with the capacitor was usually not perfect, and a small signal lasting about 30 μs usually remained. This is illustrated in Fig. 1 *b*, which is the result from 10 cycles of the P/4 procedure for a 150-mV pulse. The residual signal is small in comparison to gating current, but it is large enough to cast doubt on the first 30 μs of the recordings.

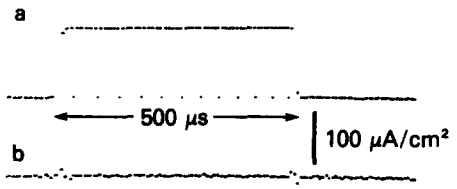

FIGURE 1. Tests of the apparatus on dummy circuits. (*a*) Temporal performance of the clamp and recording apparatus for a voltage step applied to a resistor. Rise time of the resultant signal illustrated is <20 μs (10 μs/point sampling rate). Vertical scale is arbitrary. (*b*) Test of linearity of the system on a dummy membrane. A 150-mV step was applied across a 0.047-μF capacitor. Trace illustrated is the resultant average of 10 cycles of the P/4 procedure. Subtraction is almost perfect; the first three points are erratic.

Names and compositions of all solutions are given in Table I. In most experiments $I_{Na} + I_g$ was recorded in 1/4 Na seawater, and I_g was subsequently determined after total removal of Na, addition of TTX, or both. I_g was then subtracted from $I_{Na} + I_g$ to yield the I_{Na} traces illustrated.

RESULTS

Temporal Relation between I_g and I_{Na}

Fig. 2 shows I_{Na} and I_g (after Na removal and TTX addition) recorded at several voltages from a fiber perfused with 200 TMA to eliminate potassium current. At −20 mV or −10 mV, I_g has a quick rise, complete in 40 μs, and then decays in two distinct phases. The faster phase is almost finished before I_{Na} becomes detectable. The second, slower phase continues until shortly after I_{Na} reaches its peak. This component of current, which was not well resolved in earlier records, is most clearly visible in the range between −20 mV and 0 mV and will be called the intermediate component. At more negative voltages, e.g., −40 mV, the intermediate component is too small to resolve. For large

depolarizations, positive to +20 mV, it is obscured by additional charge movement that is too slow to be associated with channel opening.

The trace at −20 mV suggests that activation is the result of one or more fast steps, giving rise to the fast component of I_g, followed by a slower one that generates the intermediate component. The additional slow charge movement seen at very positive voltages may arise from a transition between two open states (Armstrong and Bezanilla, 1977), but there is no firm evidence.

Isopotentiality along the Axon

Much of this paper is concerned with the rapid kinetics of gating current, and a first question is whether the voltage is sufficiently uniform along the axon to allow confidence in the current measurements. The amount of longitudinal

TABLE I
SOLUTIONS*

Internal solution	TMA‡-glutamate	TMA-fluoride	Trizma§ 7.0	Sucrose
	mM	*mM*	*mM*	*mM*
200 TMA	150	50	10	560

External solutions	Trizma§ 7.0	Tris base	NaCl	$CaCl_2$	$ZnCl_2$
	mM	*mM*	*mM*	*mM*	*mM*
Tris TTX‖	480	—	—	50	—
ASW	—	—	450	50	—
¼ Na	360	—	113	50	—
Tris 30 Zn	471	24	—	10	30
Tris 10 Ca	540	—	—	10	—
1:4 Na 30 Zn	353	18	116	10	30
1:4 Na 10 Ca	424	—	116	10	30

* Osmolarity of all solutions was between 950–1,000 mosM; pH was between 6.9 and 7.1.
‡ Tetramethylammonium ion.
§ Tris (hydroxymethyl) aminomethane, Sigma Chemical Co., St. Louis, Mo.
‖ Tetrodotoxin, 200 nM.

nonuniformity is strongly dependent on the membrane conductance, and a large inward Na^+ current when conductance is high should present the most severe test of uniformity. Fig. 3 shows an experiment testing for voltage nonuniformities under conditions of both high and low membrane conductance.

Internal voltage was measured simultaneously at two points separated by 5.6 mm, using the combination electrode shown in Fig. 3 *a* (see legend for details). The external voltage (V_o) was measured at only one point, in the center of the current measuring region (Fig. 3 *b*), and was subtracted from each of the two internal voltage signals to yield V_1 and V_2. The controlled voltage was V_1.

In Fig. 3 *c* and *d* the electrode was positioned with the voltage control point 5.6 mm to the right of the chamber's center. When V_1 (not illustrated) was

stepped from −70 to −20 mV, V_2 (at the center of the chamber) did not follow exactly but was always within a few millivolts of the command value. V_2 and the current generated in the central region are shown in Fig. 3 *c*.

Fig. 3 *e* shows the same procedure, after withdrawing the electrode so that the control point was at the center of the current measuring region, and V_2 was measured 5.6 mm to the left. In this case V_2 followed the command voltage rather accurately.

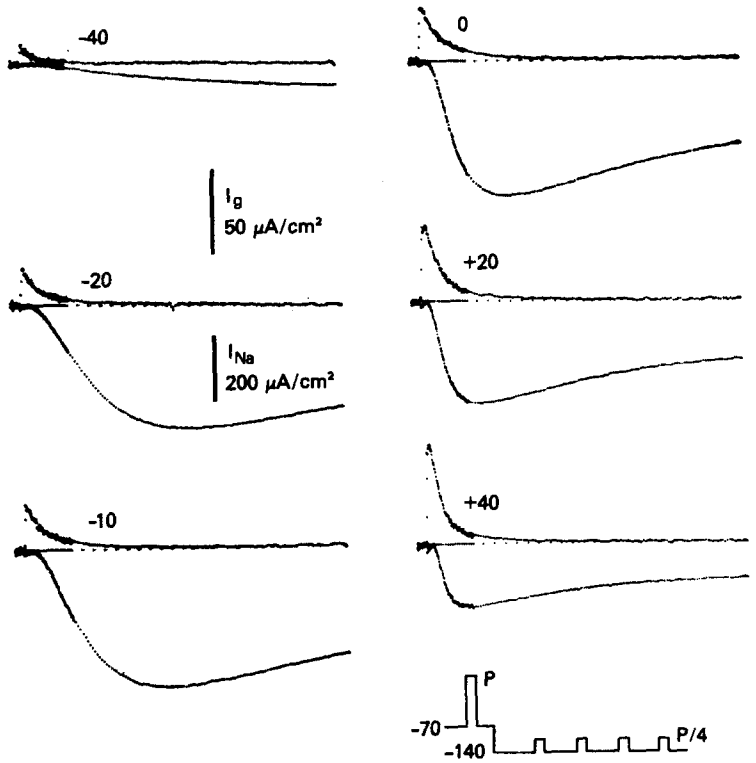

FIGURE 2. I_g (upper trace of each pair) and I_{Na} at the voltages indicated. At −40 mV only the fast component of I_g is resolvable. Between −20 and 0 mV the fast component is followed by a slower "intermediate component." This component is obscured at more positive voltages by additional very slow charge movement (+20, +4 mV). Axon SE068A; I_{Na} recorded in 1/4 Na//200 TMA, I_g in Tris TTX//200 TMA. Holding potential = −70 mV. Control pulses: P/4 from −140 mV. 8° C.

In Fig. 3 *c* and *e* there is a strong inward current and a high expectation of nonuniformity in voltage. Fig. 3 *d* and *f*, on the other hand, show V_1 and V_2 during a pulse when membrane resistance is high. V_1 was stepped from −70 to −120 mV, with the control pipette at either +5.6 mm (*d*) or 0 mm (*f*). In both cases, membrane current is very small (not illustrated). The voltage at both the control point and 5.6 mm away is a rapid step (rise time about 2 μs), regardless of the location of the control point. The conclusion is that the

membrane is isopotential during voltage steps when membrane resistance is high, as it is during gating current measurements.

I_g Has a Rising Phase for Large Depolarizations

Gating currents from two axons depolarized to 0 mV and to +50 or +60 mV are shown in Fig. 4 on an expanded time scale. In both cases the current transient for the smaller pulse shows a practically instantaneous rise and smooth decay. At +50 or +60 mV, however, there is a distinct rising phase lasting about 80 μs.

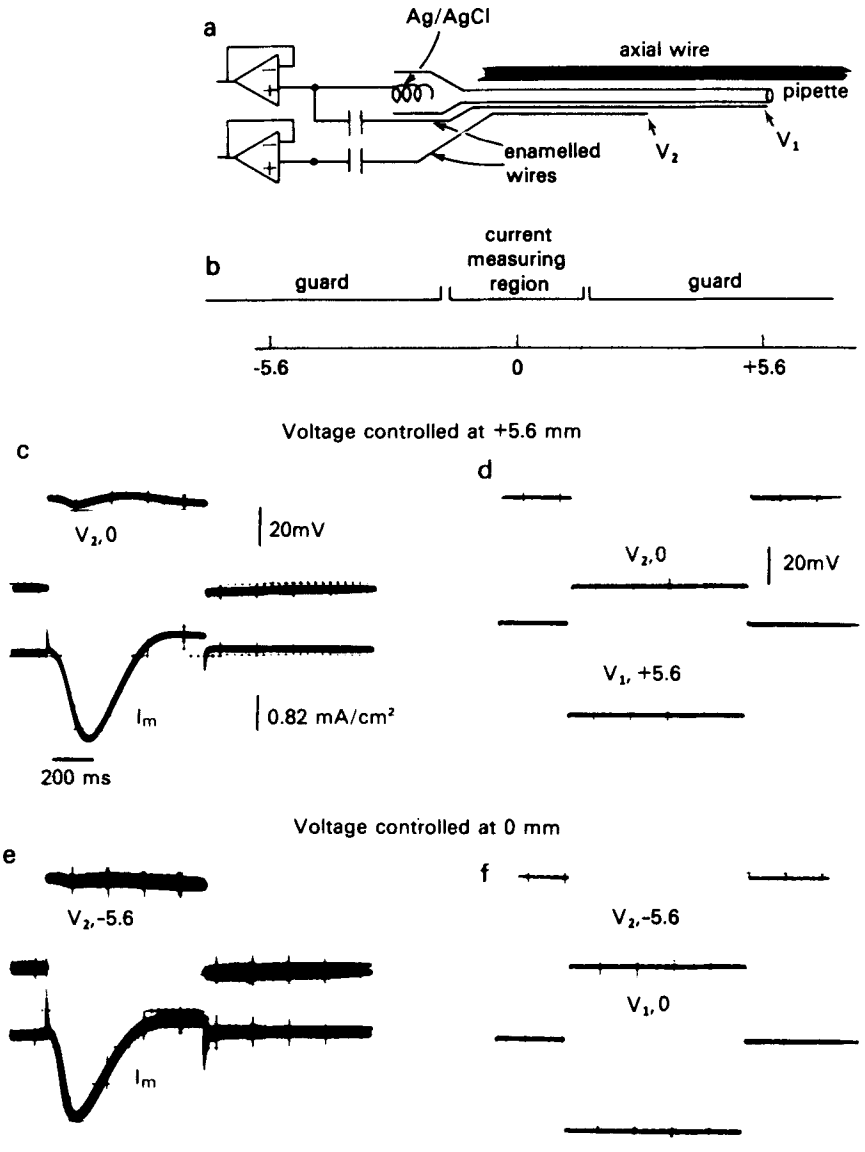

Voltage traces are also shown, for both steps in Fig. 4 *a*, and for the larger one in Fig. 4 *b*. It is clear that the membrane potential has settled to its final level before the rising phase is completed. Moreover, the shapes of the rise in gating current at these two voltages are qualitatively different, even though the voltage steps at 0 and +50 mV (Fig. 4 *a*) are very similar in shape. The lowest trace (V_m, P/4) in Fig. 4 *b* is the difference between one test (to +60 mV) and four control voltage steps for 10 cycles with the P/4 procedure,

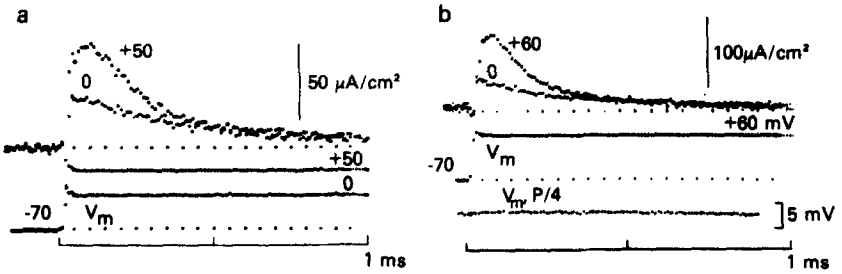

FIGURE 4. ON gating current for small and large steps of membrane potential. (*a*) Upper traces: I_g ON at 0 mV and +50 mV. Lower traces: corresponding voltage steps. Note the sharp rise in I_g ON at 0 mV and the rising phase at +50 mV that continues after the membrane potential has stabilized. Same axon as Fig. 2. (*b*) Similar records of I_g ON at 0 mV and +60 mV in another axon. Voltage trace is shown only for +60 mV. The lowest trace (V_m, P/4) shows V_m subjected to 10 cycles of the P/4 procedure (see text). Matching of test and control pulses is essentially perfect. Axon SE018G. Tris TTX//200 TMA. Holding potential −70 mV. Control pulses: P/4 from −180 mV. 8° C.

FIGURE 3 (Opposite). Isopotentiality along the axon under conditions of high and low membrane conductance. (*a*) Combination electrode for measuring intracellular voltages at two points spaced 5.6 mm apart. Two enamelled Pt wires, bare only at the tips, were attached to the outside of a pipette, which in turn was attached to a platinized axial wire. A Ag-AgCl junction in the pipette was connected to the input of a voltage follower. The Pt wire ending at the pipette mouth was connected to the same input through 0.01 μF. The output of this follower less the external voltage was the feedback signal to the clamp regardless of electrode position (see below). The other Pt wire, ending 5.6 mm away, was capacitively coupled to another voltage follower. The external voltage at the center of the chamber was subtracted from both follower outputs to yield V_1 (pipette tip) and V_2 (wire). (*b*) Scale diagram of the chamber showing relative spacings of the center of the current measuring region (0 mm) and the points ±5.6 mm away in the guard regions. The electrode assembly in *a* was advanced or withdrawn so that voltage at either 0 or +5.6 mm could be controlled. (*c*) Voltage (V_1) was controlled at +5.6 mm and stepped from −70 to −20 mV with a rise time of ~2 μs (not illustrated). Top trace shows V_2 at 0 mm. Bottom trace shows I_m in artificial seawater (ASW). V_2 is not perfectly controlled when g_m is large. (*d*) V_1 was controlled at +5.6 mm and stepped from −70 to −120 mV. V_2 (at 0 mm) is satisfactorily controlled when g_m is low. (*e*) As in *c*, but with voltage (V_1) controlled at 0 mm after moving the electrode 5.6 mm to the left. (*f*) As in *d* with V_1 controlled at 0 mm.

sampled, subtracted, and signal-averaged in exactly the same manner as were the corresponding currents. The subtraction is good, and the appearance of a rising phase with large depolarizations is therefore not due to poor matching between test and control pulses.

Tests for Distortion of I_g by Control Pulse Current

In an earlier study Armstrong and Bezanilla (1974) pointed out that with the ±P method a prominent rising phase (lasting up to 250 μs) resulted from nonlinear charge movement during the control pulse. We used several tests to assess whether control pulse current is contributing to the rising phase seen, e.g., in Fig. 4. The first was a measure of the total nonlinear charge movement in the control pulse range.

The *Q-V* curve for a typical fiber (Fig. 5 *top*) saturates at both ends, near −140 and +40 mV. (For convenience the zero current line is taken as the asymptote near −140 or −150 mV.) Some of the currents from which this curve was obtained are shown in Fig. 5 (*bottom*). The fiber was held at −70 mV, and the inward currents are for negative steps from this voltage (see diagrams). The curve shows that capacitance behaves linearly from −140 to −170 mV, but is nonlinear between −140 and −70 mV (c.f. Bezanilla and Armstrong, 1975). The control pulses for large depolarizations overlap part of this range, and the resulting nonlinear charge movement subtracts from that during the test pulse, causing an underestimate of the latter. With the P/4 procedure, the underestimate is four times the charge moved during a single control pulse.

For example, the point at +90 mV in Fig. 5 (*top*) should have added to it four times the charge at −130 mV, which was the voltage during the control pulse. The correction at several voltages (estimated from the smooth curve) is shown by the open circles in the figure. It slightly changes the shape of the *Q-V* curve, but has a negligible effect below +30 mV.

In terms of total charge movement, the contamination by control pulse current is small using the P/4 procedure. Distortion of the early time-course of I_g could nonetheless be appreciable. We used three further tests to assure ourselves that the distortion is probably not serious.

(*a*) The top trace in Fig. 6 *a* shows gating current recorded at +50 mV with control pulses from −170 to −140 mV (same axon as Fig. 5). The middle trace gives the estimated contaminating current during the control pulses obtained by taking the difference between records at −170 mV and −140 mV (from the experiment in Fig. 5 *top*) and multiplying by −4. Adding the resultant back to I_g, and thus removing the contamination, gives the noisy trace on the bottom of Fig. 6 *a*. For comparison, the uncorrected I_g trace has been superimposed. Although the rising phase is somewhat faster after correction, there is still a plateau-like initial phase. The same result was obtained in four other fibers.

(*b*) Similar information was derived in another axon by a different procedure. Fig. 6 *b* shows the effect of varying the voltage from which the control pulses originate (as indicated in the figure), again using the P/4 procedure. Gating

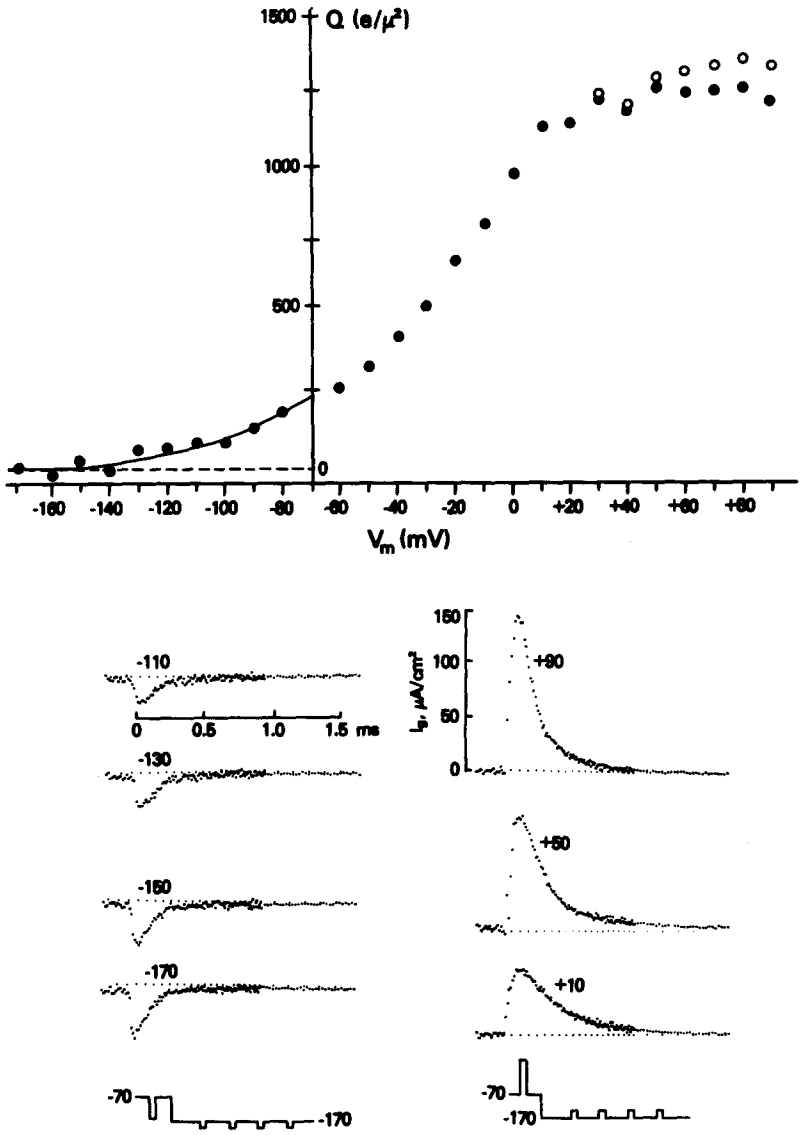

FIGURE 5. Nonlinear charge movement over the voltage range −170 mV to +90 mV. (*Top*) Steady-state voltage distribution of nonlinear charge movement. Solid points were obtained by integrating records below for 7 ms following the step. Smooth curve has been drawn by eye. Very little nonlinear charge movement can be detected negative to −130 mV. Open circles are data points corrected for the estimated nonlinear charge movement in the control pulses (see text for details). (*Bottom*) Nonlinear capacity currents (P/4 procedure) with control pulses originating from −170 mV. Membrane potential during the pulse is indicated for each trace. Axon SE058D. Tris TTX//200 TMA. Holding potential −70 mV. 8°C.

currents for all three cases are similar, but there is a tendency for the rising phase to become slightly faster and more plateau-like as the control pulse level is made more negative.

(*c*) Fig. 6 *c* shows gating currents following a depolarization to +50 mV with control pulses of either 30 or 7.5 mV amplitude, starting from −170 mV. The upper trace, with 7.5 mV control pulse, is noisy, but the rising phase is prominent as in the lower trace.

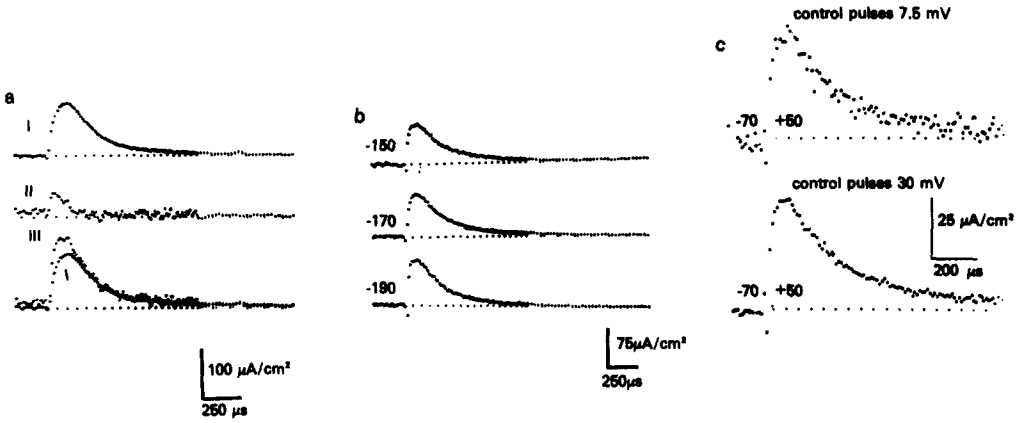

FIGURE 6. Tests for distortion by control pulse current. (*a*) I: I_g ON at +50 mV before correction. Control pulses were +30 mV starting from −170 mV. II: Contaminating current during the control pulses (see text). I and II were added together to give III, the corrected trace. The rising phase is not drastically altered by the correction. Same axon as Fig. 5. (*b*) I_g ON at +50 mV with +30 mV control pulses originating from −150, −170, or −190 mV as indicated. The rising phase is not much affected. Same axon as Fig. 4 *b*. (*c*) The effect of varying control pulse amplitude. Upper trace: I_g ON at +50 mV using +7.5 mV control pulses starting from −170 mV. The record is noisy because of the low signal-to-noise ratio with this small control pulse. Lower trace: I_g ON for same amplitude test pulse but with control pulses of +30 mV from −170 mV (P/4). There is no detectable change in the shape of I_g ON with this reduction in control pulse amplitude. Axon SE088A. Tris TTX//200 TMA. Holding potential −70 mV. 3.5° C.

I_g OFF Has a Rising Phase after a Short Pulse

Fig. 7 *a* shows I_{Na} and I_g OFF as the Na channels close at −70 mV following a 0.5-ms pulse to +50 mV. I_{Na} reaches its maximum amplitude by 40 μs and then decays abruptly. I_g, in contrast, increases in amplitude for about 80 μs before beginning to decay with a rounded time-course. As has been reported (Armstrong and Bezanilla, 1974; Meves, 1974; Neumcke et al., 1976), the decay of I_g is only a bit slower than that of I_{Na}, the respective time constants here being 321 and 239 μs.

I_g OFF traces from another experiment are shown in Fig. 7 *b* after a short pulse and after one long enough to cause Na inactivation and charge immo-

bilization. After the long pulse I_g OFF has a much sharper early time-course, and the rising phase is less pronounced. In addition there is a prominent slow phase after the long pulse, which represents the delayed return of gating charge that was immobilized by inactivation (c.f. Armstrong and Bezanilla, 1977).

I_g ON is also affected in amplitude and time-course by inactivation, as described in a subsequent section.

Zn Slows Na Activation and the Rising Phase of I_g ON, but Closing of the Channels Is Unaffected

External Zn is one of the few agents that slows Na activation kinetics, as shown by Hille et al. (1975). It also slows gating current (Armstrong and

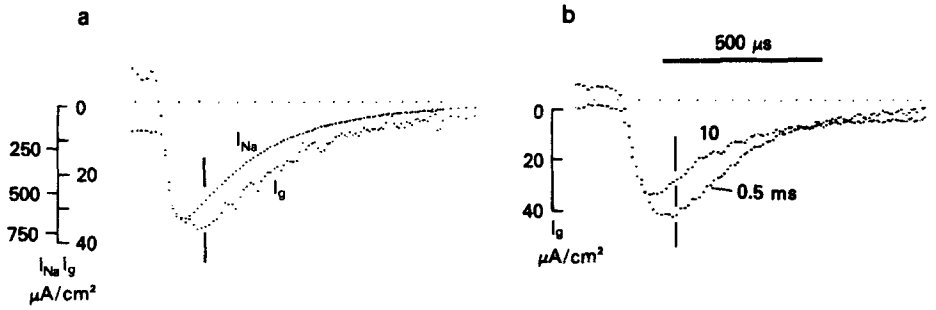

FIGURE 7. (*a*) I_g OFF and I_{Na} tails at −70 mV following a 0.5-ms depolarization to +50 mV. Vertical line is a reference mark. Axon SE098B. Tris TTX// 200 TMA. Holding potential −70 mV. Control pulses: P/4 from −150 mV. 3°C. (*b*) I_g OFF at −80 mV after a 0.5- or 10-ms pulse to +40 mV. The early phase of I_g decays more rapidly after the longer pulse. Axon SE058C. Tris 10 Ca TTX//200 TMA. Holding potential −80 mV. Control pulses: P/4 from −140 mV. 8°C.

Bezanilla, 1975). Fig. 8 *a* shows that 30 mM external $ZnCl_2$ significantly slows the rising phase of I_g, extending its duration even further beyond the settling time of the clamp (c.f. Fig. 4). Zn also depresses the peak amplitude of I_g, slows its decay (Fig. 8 *a*), and slows the activation of I_{Na} (Fig. 8 *b*). For large depolarizations, such as that shown in Fig. 8, Zn produces no change in total gating charge moved, but does cause a steady-state g_{Na} block of 20–35%. To facilitate comparison, the Zn trace was scaled up by a factor of 1.25 in Fig. 8 *b*.

Unexpectedly we found that Zn has little or no effect on channel closing. Fig. 8 *c* and *d* show I_g and I_{Na}, respectively, at −100 mV following a strong, brief depolarization. Traces in Zn have been superimposed on the zincless traces. To facilitate comparison, I_{Na} in Zn (Fig. 8 *d*) was scaled by a factor of 1.5 to account for the g_{Na} blocking action of Zn during the pulse.

The definite slowing of activation by Zn and its negligible effect on channel closing seems incompatible with the hypothesis that Zn simply shifts the g_{Na}

activation curve along the voltage axis by altering surface charge density. This was examined further by attempting to superimpose I_g ON records with and without Zn at different voltages. For example, in Fig. 8 *e* I_g ON at +60 mV in Zn (same trace as in Fig. 8 *a*) superimposes fairly well on that at +40 mV in the absence of Zn. Thus, addition of 30 mM $ZnCl_2$ is roughly equivalent to making the voltage during this step more negative by about 20 mV.

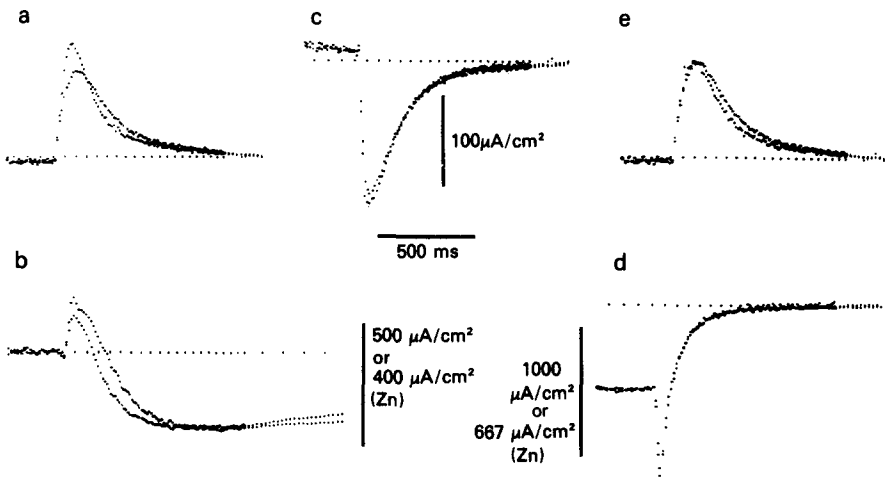

FIGURE 8. Effect of 30 mM external $ZnCl_2$ on the kinetics of I_g (*a*, *c*, *e*) and I_{Na} (*b*, *d*). (*a*) I_g ON at +60 mV before (larger amplitude trace) and during exposure to Zn. Zn slows the rising phase, decreases the peak amplitude, and slows the decay of I_g. Axon SE058B. Tris 10 Ca or Tris 30 Zn//200 TMA. Holding potential −80 mV. Control pulses: P/4 from −130 mV. 8° C. (*b*) I_{Na} + I_g with (rightmore) and without Zn. Axon was treated with internal pronase to destroy Na inactivation. The 400 μA/cm² calibration applies to the Zn trace (see text). Axon AU188D. 1/4 Na 10 Ca or 1/4 Na 30 Zn//200 TMA. Holding potential −80 mV. Control pulses: P/4 from −120 mV. 8° C. (*c*) I_g OFF at −100 mV following a 0.5 ms pulse to +50 mV before (smaller amplitude trace) and during exposure to Zn. Same axon as *a*. (*d*) I_{Na} (+ I_g) tails at −100 mV following a 1.2 ms pulse to 0 mV before and during Zn. The 667 μA/cm² calibration applies to the Zn trace. The time-course of the tail current is unaltered by Zn. Same axon as *b*. (*e*) Comparison of I_g ON with (+60 mV) and without (+40 mV) Zn. See text. Same axon as *a*.

A similar procedure applied to I_g OFF in a number of axons showed that Zn has no consistent effect on either I_{Na} or I_g as channels are closing. The action of Zn is therefore more complex than simply a shift in the steady-state voltage dependence of activation by alteration of surface charge. An alternate explanation is suggested in the discussion, and a detailed analysis of zinc's effects on activation is in preparation.

Prepulses That Produce Na Inactivation Abolish the Rising Phase of I_g

Armstrong and Bezanilla (1974, 1975, 1977) and Meves and Vogel (1977 *a, b*) have reported that inactivation of sodium conductance during a long depolarization "immobilizes" a large part of gating charge. Another effect of depolarizing prepulses not specifically discussed by these authors is exerted on the shape of the rising phase. The effect, illustrated in Fig. 9, is like that on I_g OFF after a long pulse described above, but is rather more pronounced.

Trace *a* in Fig. 9 shows I_g ON recorded with the usual procedure (pulse sequence *a*), whereas trace *b* is the inactivation or immobilization resistant charge after a prepulse (sequence *b*; see legend for details). The prepulse reduces total charge movement, abolishes the rising phase, and selectively reduces the slow component. Kinetics of the inactivation resistant charge are

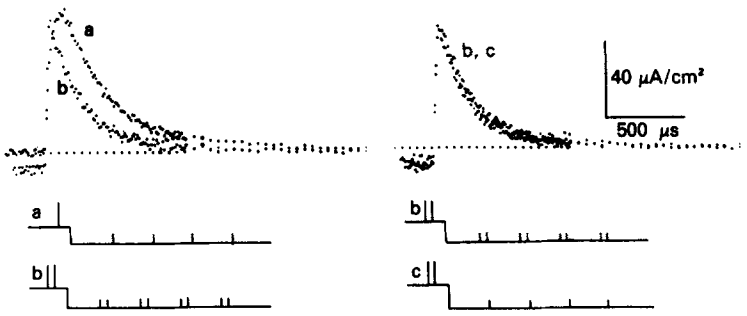

FIGURE 9. Effect of a long depolarizing prepulse that produces Na inactivation on the kinetics of I_g ON. (*a*) I_g ON at +50 mV with no prepulse. The rising phase lasts for ~100 μs. (*b*) I_g ON following a 7-ms prepulse to +50 mV and a 0.8-ms recovery period at −70 mV (pulse sequence *b*). The rising phase is abolished, and the subsequent decay is approximately exponential. (*c*) I_g ON with the same pulse protocol as in *b*, but with prepulses omitted before the control pulses (pulse sequence *c*). Traces *b* and *c* are not detectably different, showing that the prepulse effect is not exerted via changes in control pulse currents. Same axon as Fig. 8 *a*.

thus greatly simplified. For convenience this experiment was done in the presence of 30 mM external Zn to make the rising phase more prominent. Similar results have been obtained without Zn.

For trace *c* in Fig. 9 the prepulse was omitted before the control pulses (sequence *c*). Records *b* and *c* are indistinguishable, showing that the prepulse effect on the rising phase is not due to an effect on control pulse currents.

As noted in a previous section, I_g OFF has a rising phase similar to that of I_g ON after a short pulse, but not after a long one. This effect occurs with a time-course very similar to the development of charge immobilization and Na inactivation (Armstrong and Bezanilla, 1977; see their Fig. 2).

Reappearance of the rising phase of I_g ON following a depolarizing prepulse occurs roughly in parallel with the removal of I_g immobilization and Na

inactivation. Fig. 10 *a* shows gating current (lefthand trace) and I_{Na} at +60 mV with no prepulse, and the initial plateau phase of I_g ON is apparent. I_{Na} was obtained with the same pulse protocol before adding TTX. I_g and I_{Na} records following a 15-ms prepulse to +60 mV and recovery at −70 mV for the durations indicated are shown in Fig. 10 *b–e*. As the recovery period lengthens, (*a*) the initial phase of I_g ON becomes more plateau-like (i.e., the rising phase develops); (*b*) the intermediate component of I_g (see above) reappears; and (*c*) I_{Na} reappears.

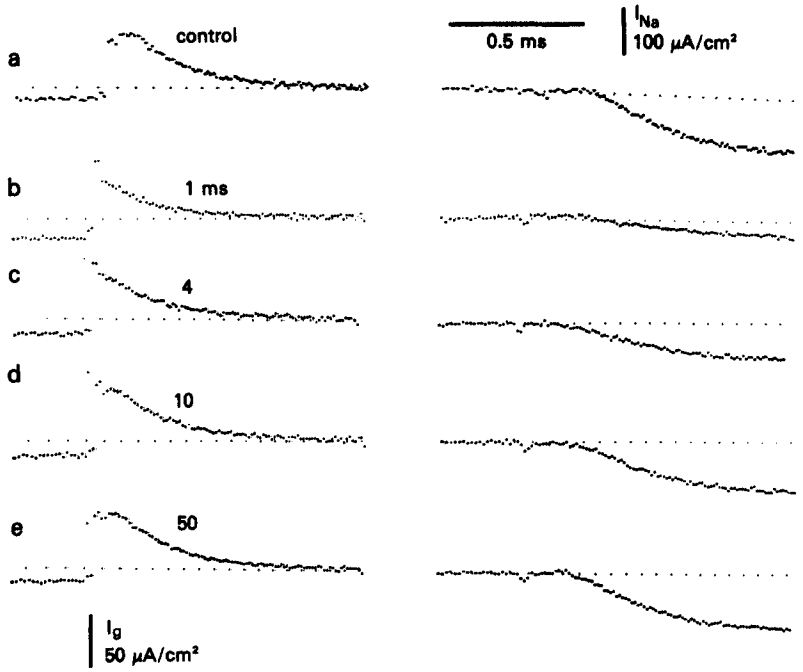

FIGURE 10. Recovery of I_g ON and I_{Na} from the effects of a long depolarizing prepulse. (*a*) I_g ON (left) and I_{Na} at +60 mV with no prepulse (*a*), or (*b–e*) following a 15-ms prepulse to 60 mV. Between pre- and test pulse, V_m was held at −70 mV for the time indicated. With the shortest recovery interval (*b*, 1 ms) the rising phase of I_g ON is abolished, and I_{Na} is small. As the recovery period lengthens, the rising phase and the intermediate component of I_g (see text) reappear along with I_{Na}. Same axon as Fig. 7 *a*.

The rising phase thus disappears and reappears with about the same time-course as development and removal of both I_g immobilization and Na inactivation, and the effect is not due to changes in nonlinear currents during the control pulses. These observations are explored more fully in the next section.

DISCUSSION

Recorded gating current is the difference of currents during test and control pulses, and it is logically impossible to resolve this combination into its

components with absolute certainty (c.f. Almers, 1978). With this preface in mind, we feel the following points about the time-course of I_g are reasonably well established by this paper.

(1) I_g has an initial plateau or rising phase that is not a machine artifact and is probably not due to nonlinear charge movement during the control pulses. Briefly, the evidence is: (*a*) A rising phase is seen only with large voltage steps, even though the voltage settles equally rapidly for small and large steps. (*b*) I_{Na} tails have a sharper rise than does I_g OFF. (*c*) External Zn ions prolong the rising phase, and (*d*) an inactivating prepulse eliminates it. (*e*) The rising phase is not much altered (if at all) by using control steps of different amplitude, or by varying the voltage from which the control pulses originate.

Nonner et al. (1978) observed a fast rising phase (<30 μs) for I_g ON (but not for I_g OFF) in frog node of Ranvier and concluded that it probably resulted from contamination by inward current during the control pulses. Their records were obtained with symmetrical pulses that originated from −97 mV. In other experiments, they detected nonlinear current negative to −97 mV and concluded this current was responsible for the rising phase. We agree fully that there is nonlinear capacity current between −97 and roughly −120 mV, but our method avoids this region, and our records nonetheless have a rising phase. Further, their analysis does not provide an explanation for the fact that they (and we) saw a rising phase only for large pulses.

(2) The second major point is that over the voltage range from about −30 to 0 mV, I_g ON has a fast phase that precedes the conductance change and a less rapid one (the intermediate component) that is roughly proportional to the time derivative of g_{Na}. It seems inescapable that activation involves one or, more likely, several fast steps, which generate the fast phase of I_g, followed by a slower step which generates the intermediate component.

(3) For steps to +10 mV or more positive, there is additional charge movement (the slow component) that seems too slow to be associated with activation of Na channels.

(4) I_g OFF has a rounded time-course and a decay phase at −70 mV that is almost as rapid as the fall of the g_{Na}.

(5) Finally, when the channels are inactivated, I_g ON approximates a single exponential with an almost instantaneous rise (i.e, faster than 30–40 μs).

These results can be thought of in terms of the kinetic diagram in Fig. 11, which is a simplification of one given earlier by Armstrong and Bezanilla (1977). The steps along the horizontal axis represent changes in the activation gate from "fully closed" at the left (x_6) to the conducting state ($x\dagger$) at the extreme right. The horizontal steps are voltage dependent and are associated with gating charge movement, as indicated by the symbols Q_1 and Q_x. The vertical steps represent movement of an inactivating particle into (up) or out of (down) its receptor. The inactivation steps are not significantly voltage dependent and generate no detectable gating current. The activation gate is open to the right of the vertical dashed line; the inactivation gate is open below the horizontal dashed line. Both gates must be open for the channel to

conduct, and this is the case only for x_1^*, the single conducting state. This scheme is adequate for present purposes, but fails to reproduce the voltage dependence of recovery from inactivation (c.f. Armstrong and Bezanilla, 1977).

As noted, all steps along the horizontal axis generate gating current. Necessary conditions for a rising phase are that some of the steps to the right have faster rate constants than do the ones at the left, and/or they have more gating charge movement per step. The intermediate component of I_g seen near −20 mV suggests that one of the later steps must be relatively slow. Our results can be explained by postulating that the last step in opening a channel, $x_2 \rightleftharpoons x_1^*$, is substantially slower than the preceeding steps, has more charge movement associated with it, and is therefore more voltage dependent with regard to kinetics and equilibrium constant. This step generates the intermediate component of I_g, which would have the time-course of dg_{Na}/dt if there were no inactivation.

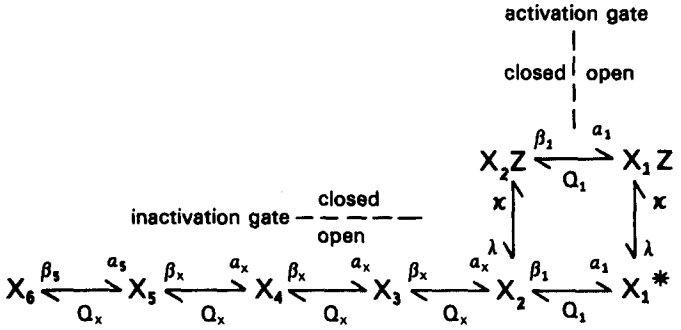

FIGURE 11. State diagram of a sodium channel. See text for details.

Calculations of g_{Na} and I_g were performed using this model, with the initial condition that all of the channels are in state x_6 at rest (−70 mV). (This is an approximation, for a few of the channels would be in the other states at −70 mV.) $x_1^*(t)$, which is directly proportional to conductance, was calculated by numerically integrating the eight first-order differential equations that describe the scheme drawn above. Gating current for each step was calculated from an equation of the type:

$$I_{gx_2 \rightleftharpoons x_1} = Q_1\left(\frac{dx_1^*}{dt}\right) = Q_1(\alpha_1 x_2 - \beta_1 x_1^*), \tag{1}$$

and total I_g was the sum of that for all steps. For simplicity in the initial stages of fitting, it was assumed that charge movement and rate constants for all of the fast steps (all those to the left of x_2) were the same (Q_x, α_x, β_x). Ultimately, the $x_6 \rightleftharpoons x_5$ step was made slightly slower, but the original charge, Q_x, was retained.

We assumed the following relations for calculating the equilibrium constants K_1 and K_x as functions of voltage:

$$K_1 = \frac{\alpha_1}{\beta_1} = \exp\left[\frac{Q_1(V_m - V_1)}{25 \text{ meV}}\right]; \quad (2)$$

$$K_x = \frac{\alpha_x}{\beta_x} = \exp\left[\frac{Q_x(V_m - V_x)}{25 \text{ meV}}\right]. \quad (3)$$

V_1 and V_x are the voltages at which K_1 and K_x, respectively, are equal to one. Both V_1 and V_x are about −30 mV, slightly negative to the midpoint of the Q-V distribution. Q_1 and Q_x were selected so that g_{Na} amplitude was correctly predicted at all voltages. It turned out that the total potential energy change for all steps taken together was 6 meV per millivolt change of membrane potential, precisely the original estimate of Hodgkin and Huxley (1952).

Using these relations and assumptions, the rate constants and Q_1 and Q_x were determined by an informal method of successive approximations. Representative calculations using the parameters in Table II are shown in Fig. 12. The model correctly predicts most kinetic features of g_{Na} and I_g including the fast and intermediate components of I_g, the rising phase of I_g, and the effects of prepulses and of Zn on g_{Na} and I_g.

TABLE II
PARAMETERS FOR CALCULATIONS

V_m	α_1	α_{2-4}	α_5	β_1	β_{2-4}	β_5	κ	λ	Fig. ref.
I_g ON									
−20	0.6	10	7.7	0.257	7.14	5.5	0.1	0.01	12 *a*
+10	2.3	14	10.8	0.089	3.01	2.33	0.12	0.012	12 *b*
+50	4.5	22	17	0.007	0.955	0.735	0.15	0.015	12 *c*
I_g OFF									
−70*	0.137	7.6	5.87	3.2	40	30.9	0.1	0.01	12 *d, e*
Inactivation effect									
+60	6	30	23	0.004	0.87	0.62	0.15	0.02	13 *a*
+60‡	—	—	—	—	—	—	—	—	13 *b*
Zn effect									
+60	7	30	23	0	1	0.77	0.25	0.02	13 *c*
+60§	—	—	—	—	—	—	—	—	13 *d*

Initial condition for all calculations (except *, ‡, §) is $x_6 = 1.0$. V_1 and V_x in Eqs. 2 and 3 are −30.6 and −28.4 mV, respectively. $Q_1 = 2$ e and $Q_x = $ e.

* Initial conditions calculated from I_g ON at +50 mV out to 1 ms. $x_{1z} = 0.107$, $x_{2z} = 0.0032$, $x_1 = 0.859$, $x_2 = 0.029$, $x_3 = 0.0016$, $x_4 = x_5 = {}_6 \simeq 0$.

‡ After prepulse. Initial conditions changed to $x_6 = 0.35$, $x_{2z} = 0.65$, as judged from I_{Na} traces in Fig. 10 *a, b*.

§ Zn-induced state (x_{Zn}) added to the left of x_6. $\alpha_6 = 40$, $\beta_6 = 26.7$ (see text).

Time-Course of g_{Na} and I_g

Fig. 12 *a–c* shows experimental traces of g_{Na} and I_g ON together with the calculated conductance (x_1^*) and gating current at three widely spaced voltages. The fits to the conductance traces are reasonably good, except that the calculated rise is slightly too quick. Another fast step would probably be helpful in remedying this.

Fits to the early part of I_g ON are very good at all voltages. In particular, calculated I_g has a rising phase at +50 mV but not at −20 mV, in agreement with experimental observation. At +10 and +50 mV the model does not fit the slow component of I_g, another suggestion that this component is too slow to be associated with activation.

The fit to g_{Na} and I_g as the channels close (Fig. 12 *d* and *e*) is qualitatively correct in that I_g has a more rounded time-course than does g_{Na}, and the final rate of decay of g_{Na} and I_g is about the same.

Table II shows that the rate constants behave in a reasonable way as V increases: α_1 and α_x increase, and β_1 and β_x decrease smoothly. As noted, the

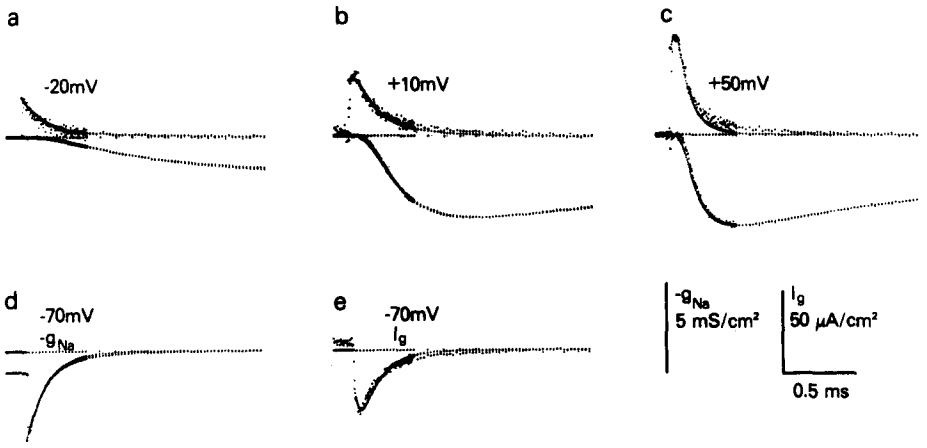

FIGURE 12. Comparison of experimental and calculated I_g and g_{Na}. Calculations were based on the model of Fig. 11, using the parameters and initial conditions given in Table II. g_{Na} is taken as I_{Na} divided by $(V - V_{Na})$ with V_{Na} = +88 mV. (*a*, *b*, *c*) Experimental and calculated I_g ON (upper pair of records) and g_{Na} (lower pair) at the indicated voltages. (*d*, *e*) Experimental and calculated g_{Na} (*d*) and I_g (*e*) as channels close at −70 mV following a 1-ms pulse to +50 mV. Same axon as Fig. 7 *a*.

ratios α_1/β_1 and α_x/β_x were calculated from Eqs. 2 and 3, a restriction that made it somewhat surprising that the conductances fit as well as they do. Still better fits could probably be obtained by small adjustments of Q_1, Q_x, or other parameters: we exhausted our patience but not the possibilities of the model. The rate constants κ and λ change very little with voltage, e-fold for roughly 175 mV (c.f. Bezanilla and Armstrong, 1977), compatible with the hypothesis that the inactivation step involves little if any measurable charge movement.

Effect of Inactivation

At the end of a long depolarizing step most of the channels are inactivated and in state x_1z. On repolarization the likely step is $x_1z \rightarrow x_2z$, which is much more rapid than $x_1z \rightarrow x_1^*$. The transition from x_1z to x_2z generates the

inactivation resistant component of gating current, which is exponential since only one step is involved. Thus I_g tails seen after a long pulse do not have the hook seen after shorter steps. Experimentally it is impossible to observe this component without some contamination from charge movement associated with other steps.

In Figs. 9 and 13 *b* the membrane was repolarized for 0.8 or 1 ms following a long depolarizing prepulse, and a second depolarizing step was then applied.

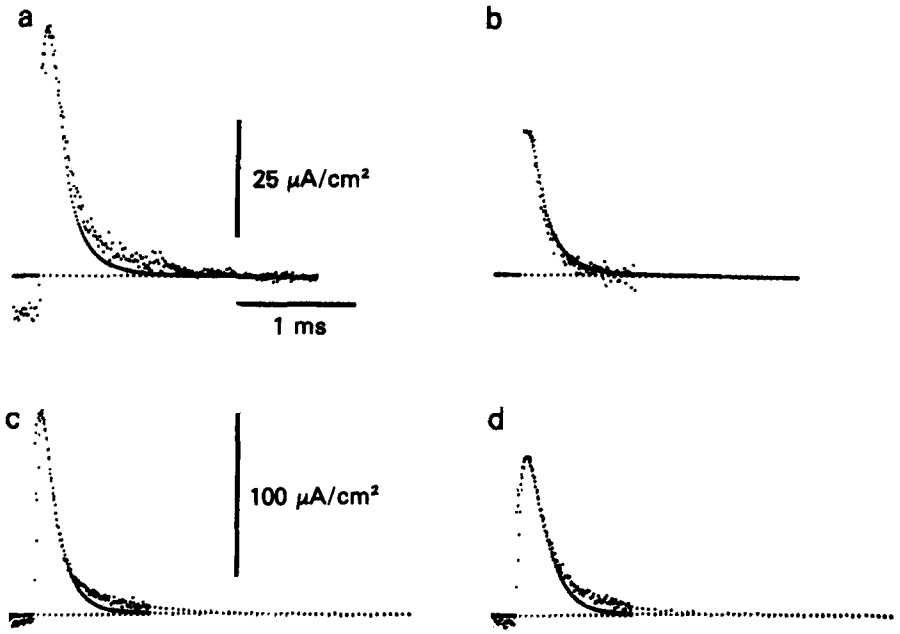

FIGURE 13. Experimental and calculated I_g ON showing the effects of a depolarizing prepulse (*a, b*) or external Zn (*c, d*). Parameters initial conditions are given in Table II. (*a*) I_g ON at +60 mV. (*b*) I_g ON at +60 mV following a 15-ms prepulse to +60 mV and 1-ms recovery at −70 mV. Same experiment as in Fig. 10 *a, b*. (*c*) I_g ON at +60 mV. (*d*) I_g ON at + 60 mV in the presence of 30 mM $ZnCl_2$. Same experiment as in Fig. 8 *a*.

At the beginning of the second step, most of the channels (about two thirds) are in state x_2z, and most of the remainder are in state x_6. During the second step the channels in x_2z move to x_1z, generating an exponential current, which is added to the more complicated current generated by the channels moving from x_6 to x_7^*. Simulations of the experiment in Fig. 13 *a* and *b* are given by the smooth curves. In both experiment and simulation the rising phase of I_g is almost eliminated following a prepulse.

Zn Effect

A possible explanation for the action of Zn is that it binds to a negatively charged group that is part of the gating apparatus. The negative group is at

the outer surface of the membrane and accessible to external Zn only when the channel is fully closed, in state x_6. On depolarization the extra step required as Zn dissociates, $x_{Zn} \rightleftarrows x_6$, slows activation. Once the channel has progressed to x_5, the Zn-binding group has migrated inward and become inaccessible to Zn, which has no further effect on kinetics. Specifically, there is no effect on channel closing (see Fig. 8 *c* and *d*). Calculations of I_g ON based on this model are shown in Fig. 13 *c* and *d*, together with experimental traces which are well fitted except for the slow component. Parameters of the fit are given in Table II. It is clear without calculation that I_g OFF will be unaffected.

I_{Na} during Recovery from Inactivation

Experimentally there is no detectable sodium current as channels recover from inactivation (Armstrong, 1978). The model accounts for this because the recovery path, $x_1 z \rightarrow x_2 z \dashrightarrow x_6$, bypasses the conducting state.

The model thus has qualitatively correct behavior in all instances tested. Its most important feature is the postulate that the last step is the slowest and most voltage dependent: we regard this as established and inescapable. There are two other significant conclusions. First, all of the early part of gating current is accounted for as being essential to activation of Na channels. Second, there is a slow component that clearly is not explained by the model. Conceivably this component is associated with a transition to a second open state (Armstrong and Bezanilla, 1977). Another possibility is that it is the early phase of gating current from K channels, which may, like Na channels, activate in several fast steps followed by a slow one. This seems somewhat unlikely, since the slow component seems not greatly altered in circumstances where the K channels have ceased to function[1] but it remains a possibility.[2]

Supported by grant 12547 from the U.S. Public Health Service.

Received for publication 6 July 1979.

REFERENCES

ALMERS, W. 1978. Gating currents and charge movements in excitable membranes. *Rev. Physiol. Biochem. Pharmacol.* **82**:96–190.

ARMSTRONG, C. M. 1978. Intramembranous charge movement and control of cellular functions by membrane voltage. *In* Biophysical Aspects of Cardiac Muscle. M. Morad, editor. Academic Press, Inc. New York. 27–29.

ARMSTRONG, C. M., and F. BEZANILLA. 1973. Currents related to movement of the gating particles of the sodium channels. *Nature (Lond.)*. **242**:459–461.

ARMSTRONG, C. M., and F. BEZANILLA. 1974. Charge movement associated with the opening and closing of the activation gates of the Na channels. *J. Gen. Physiol.* **63**:533–552.

[1] Almers, W., and C. M. Armstrong. 1980. Survival of K^+ permeability and gating currents in squid axons perfused with K^+-free media. *J. Gen. Physiol.* In press.

[2] Gilly, W. F., and C. M. Armstrong. Gating current and K channels in the giant axon of the squid. Manuscript submitted for publication.

ARMSTRONG, C. M., and F. BEZANILLA. 1975. Currents associated with the ionic gating structures in nerve membrane. *Ann. N.Y. Acad. Sci.* **264:**265–277.

ARMSTRONG, C. M., and F. BEZANILLA. 1977. Inactivation of the sodium channel. II. Gating current experiments. *J. Gen. Physiol.* **70:**567–590.

BEZANILLA, F., and C. M. ARMSTRONG. 1975. Properties of the sodium channel gating current. *Cold Spring Harbor Symp. Quant. Biol.* **40:**297–304.

BEZANILLA, F., and C. M. ARMSTRONG. 1977. Inactivation of the sodium channel. I. Sodium current experiments. *J. Gen. Physiol.* **70:**549–566.

GOLDMAN, L., and C. L. SCHAUF. 1972. Inactivation of the sodium current in Myxicola giant axons. Evidence of coupling to the activation process. *J. Gen. Physiol.* **59:**659–675.

HILLE, B. A., A. WOODHULL, and B. I. SHAPIRO. 1975. Negative surface charge near sodium channels of nerve: divalent ions, monovalent ions and pH. *Phil. Trans. R. Soc. Lond. B. Biol. Sci.* **270:**301–318.

HODGKIN, A. L., and A. F. HUXLEY. 1952. A quantitative description of membrane current and its application to conduction and excitation in nerve. *J. Physiol. (Lond.).* **117:**500–544.

HOYT, R. C. 1965. The squid giant axon: mathematical models. *Biophys. J.* **3:**399–431.

KEYNES, R. D., and E. ROJAS. 1973. Characteristics of the sodium gating current in the squid giant axon. *J. Physiol. (Lond.).* **233:**28–30P.

KEYNES, R. D., and E. ROJAS. 1974. Kinetics and steady state properties of the charged system controlling sodium conductance in the squid giant axon. *J. Physiol. (Lond.).* **239:**393–434.

MEVES, H. 1974. The effect of holding potential on the asymmetry currents in squid giant axons. *J. Physiol. (Lond.).* **243:**847–867.

MEVES, H., and W. VOGEL. 1977 *a*. Inactivation of the asymmetrical displacement current in giant axons of *Loligo forbesi*. *J. Physiol. (Lond.).* **267:**377–393.

Meves, H., and W. VOGEL. 1977 *b*. Slow recovery of sodium current and gating current from inactivation. *J. Physiol. (Lond.).* **267:** 395–410.

NEUMCKE, B., W. NONNER, and R. STÄMPFLI. 1976. Asymmetrical displacement current and its relation with the activation of sodium current in the membrane of frog myelinated nerve. *Pflügers Arch. Eur. J. Physiol.* **363:**193–203.

NONNER, W., E. ROJAS, and R. STÄMPFLI. 1978. Asymmetrical displacement currents in the membrane of frog myelinated nerve: Early time course and effects of membrane potential. *Pflügers Arch. Eur. J. Physiol.* **375:**75–85.